

Protected gap closing in Josephson junctions constructed on Bi₂Te₃ surface

Zhaozheng Lyu,¹ Yuan Pang,¹ Junhua Wang,¹ Guang Yang,¹ Jie Fan,¹ Guangtong Liu,¹ Zhongqing Ji,¹ Xiunian Jing,^{1,2}
Changli Yang,^{1,2} Fanming Qu,^{1,3} and Li Lu^{1,2,*}

¹Beijing National Laboratory for Condensed Matter Physics, Institute of Physics, Chinese Academy of Sciences; School of Physical Sciences, University of Chinese Academy of Sciences, Beijing 100190, People's Republic of China

²Collaborative Innovation Center of Quantum Matter, Beijing 100871, People's Republic of China

³CAS Center for Excellence in Topological Quantum Computation, University of Chinese Academy of Sciences, Beijing 100190, People's Republic of China



(Received 14 March 2016; published 4 October 2018)

On the road of searching for Majorana zero modes (MZMs) in topological insulator-based Josephson junctions, a highly sought signature is the protected full transparency of electron transport through the junctions due to the existence of the MZMs, associated with complete gap closing between the electronlike and holelike Andreev bound states (ABSs). Here we present direct experimental evidence of gap closing and full transparency in single Josephson junctions constructed on the surface of three-dimensional topological insulator (3D TI) Bi₂Te₃. Our results demonstrate that the two-dimensional (2D) surface of 3D TIs provides a promising platform for hosting and manipulating MZMs.

DOI: [10.1103/PhysRevB.98.155403](https://doi.org/10.1103/PhysRevB.98.155403)

I. INTRODUCTION

Recently, much attention has been focused on searching for Majorana zero modes (MZMs) in condensed matter systems [1–4]. These MZMs, which could be used as topologically protected qubits, are expected to occur at the boundaries of *p*-wave-like superconductors. Experimentally, a number of peculiar phenomena were observed and believed to relate to the occurrence of MZMs, including the appearance of a zero-bias conductance peak (ZBCP) [5–13], the signatures of fractional Josephson effect [14,15], and the emerging of skewed current-phase relations (CPRs) in related Josephson devices [16–19]. In the presence of MZMs, however, the ZBCP is expected to be completely quantized, and the charge transport fully transparent (i.e., perfect Andreev reflection) in related devices [20–28]. While the complete quantization of ZBCP has been observed very recently [29], the complete closing of minigap between the electronlike and holelike ABSs, as a signature of fully transparent charge transport, has not yet been strictly proven.

In this work we studied the magnetic flux-dependent evolution of the local induced minigap in single Josephson junctions constructed on the surface of a three-dimensional topological insulator Bi₂Te₃. Our results lead to the conclusion that the minigap undergoes complete closing.

II. EXPERIMENTAL METHOD AND RESULTS

The devices used in this work were fabricated on exfoliated Bi₂Te₃ flakes of ~100 nm in thickness. Two “T”-shape Pb pads were sputtering deposited on the surface of the flakes to define a superconductor-TI-superconductor (S-TI-S) Josephson junction. Three nonsuperconducting Pd electrodes were

e-beam evaporated and introduced to the Bi₂Te₃ surface at the left, right, and center of the junction [marked by A, B, and C in Fig. 1(a), respectively] for detecting the local electron states. The contacting area of each Pd electrode is defined by the windows through an overexposed polymethyl methacrylate (PMMA) layer which was fabricated prior to the deposition of the Pd electrodes, for the purpose to isolate the arms of the Pd electrodes from the Pb junction underneath. The other two Pd electrodes away from the junction were added for transport measurements. The electron transport measurements with configurations illustrated in Fig. 1(b) were performed by using a lock-in amplifier technique, down to 20 mK in a dilution refrigerator. The electron temperature of the system is slightly higher, ~50 mK, known from the numerical simulations for the experimental data (will be shown later).

A. The Josephson supercurrent between the two Pb electrodes

First, we measured the differential resistance $dV/dI_{JJ\text{bias}}$ between the two Pb electrodes of a Pb-Bi₂Te₃-Pb Josephson junction (device 1), as functions of magnetic field B and bias current $I_{JJ\text{bias}}$ at the base temperature. The results are shown in Fig. 2, with the bias current swept from the bottom to the top. The white-colored area represents the zero-resistance state. The pattern is slightly asymmetric along the vertical direction, as is usually seen in literature for Josephson junctions of the similar type. The envelope of the zero-resistance state along the positive bias direction agrees well with the Fraunhofer pattern of critical supercurrent for Josephson junctions in the nontransparent limit (the red curve). Highly transparent Josephson junctions are known to show CPR significantly different from the 2π -period sinusoidal form [30], which will lead to an envelope of zero-resistance state different from the standard Fraunhofer pattern (for further explanation please refer to the Supplemental Material [31]). The period of the

*Corresponding author: lilu@iphy.ac.cn

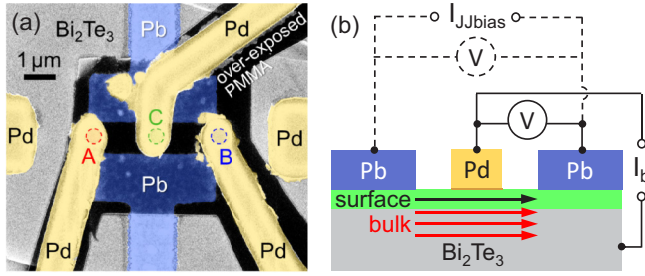


FIG. 1. (a) The false colored scanning electron microscope image of device 1. (b) A side view of the device showing that there are two supercurrents flowing through the surface and the bulk of Bi_2Te_3 . Also shown are the wiring configurations for measuring the Fraunhofer pattern (dashed lines) and the contact resistance (solid lines).

Fraunhofer pattern is $\Delta B = 2.8 \pm 0.2$ G. It corresponds to an effective junction area of $S_{\text{eff}} = \phi_0 / \Delta B = 7.14 \mu\text{m}^2$ (where $\phi_0 = h/2e$ is flux quantum, e is the electron charge, and h is the Planck constant). This estimated area is in good agreement with the geometric area of the junction $W \times H = 4 \mu\text{m} \times 1.8 \mu\text{m} = 7.2 \mu\text{m}^2$, where W is the width and H is the effective distance between the two Pb electrodes after considering flux penetration and compression [31].

B. The contact resistance in the junction area probed by Pd electrodes

Then we measured the contact resistance of the Pd electrodes by employing a three-terminal configuration as illustrated in Fig. 1(b), to probe the local electron states in the junction area. The measurement current was kept $\sim 1/1000$ of the critical supercurrent of the Josephson junction, to avoid disturbing the status of the Josephson junction. Figures 3(a)–3(c) show the 2D color plots of the contact resistance dV/dI_b on device 1 at positions A, B, and C, respectively, as functions of B and bias current I_b . In contrast to the continuous variation of the Fraunhofer pattern shown in Fig. 2, the contact resistance of all contacts exhibits sharp jumps when B is swept across

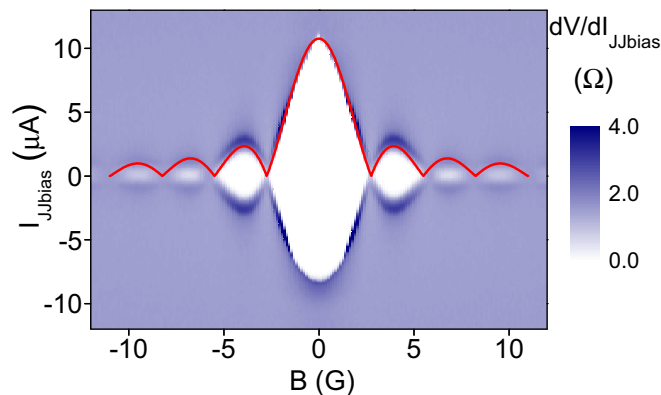


FIG. 2. The differential resistance dV/dI_{JJbias} measured between the two Pb electrodes, as functions of magnetic field B and bias current I_{JJbias} at ~ 20 mK. The red line represents the expected Fraunhofer envelope of the zero-resistance state in the nontransparent limit.

the nodes of the Fraunhofer pattern. These sharp jumps can also be clearly seen from the horizontal line cuts of the 2D plots. The line cuts of Figs. 3(a) and 3(b) at $I_b = 0$, plotted in Figs. 3(d) and 3(e), respectively, show a skewed B dependence followed by abrupt jumps. And the line cut of Fig. 3(c) at $I_b = 0$, plotted in Fig. 3(f), shows a square-shape B dependence before rectified by the Fraunhofer-like envelope.

In Figs. 3(g)–3(i) we plot the vertical line cuts taken at different B in the corresponding 2D plots. It can be seen that a gaplike structure on dV/dI_b curves undergoes sudden opening/closing with varying B at the Fraunhofer nodes (i.e., jumping between curves with most pronounced gap structures to least pronounced ones). We will show later that the remaining tiny signature of gap after gap closing, i.e., those on the black and the orange curves in Figs. 3(g)–3(i), is caused by the finite size effect of the Pd electrodes.

The contact resistance of Pd electrodes in device 1 was higher than the quantum unit $h/2e^2 = 12.9$ k Ω , indicating that the measurement was in the tunneling regime, so that the results reflect mostly the information of the electron density of states underneath. We have fabricated and measured more than ten devices. Similar results were obtained even when the contact resistance of Pd electrodes was in a range below the quantum unit $h/2e^2$, presumably because multiple tunneling channels shunt together in the contacting area. Figures 3(j)–3(o) give such an example.

Gap closing can be most clearly seen in the main frame and the inset of Fig. 3(o), where the normal-state value of dV/dI_b can be firmly determined and is represented by the horizontal blue line. It can be seen that $\sim 95\%$ of the peak height suddenly vanishes upon gap closing, i.e., from 147 Ω at 3.3 G to 8 Ω at 3.4 G.

Gap closing can also be seen in Figs. 3(d)–3(i), and 3(m). The line cuts in these plots, which represent the field-dependent peak height of the dV/dI_b curves, approach to the normal-state values at their oscillatory minimums.

III. DISCUSSIONS

A. The phase dependence of superconducting minigap

That the contact resistance dV/dI_b and the Fraunhofer pattern of supercurrents share the same oscillation period implies that the dV/dI_b oscillation is controlled by the same phase difference φ across the junction. It is known for S-N-S type Josephson junctions (where N denotes normal metals) that the backwards and forwards Andreev reflections between the two S-N interfaces lead to the formation of ABSs in the N. The minigap Δ in the junction area, which is the level spacing between the lowest-energy electronlike and holelike ABSs, shall oscillate with φ [32]:

$$\Delta = \Delta_0 \sqrt{1 - D \sin^2(\varphi/2)}, \quad (1)$$

where Δ_0 is the maximal value of the minigap, D is the total transmission coefficient of the junction, including those of the two S-N interfaces and that of the N part.

The oscillation of Δ with varying φ is depicted in Fig. 4. It can be seen that the more transparent the junction is, the more oscillatory the minigap will be. But it is very difficult to reach

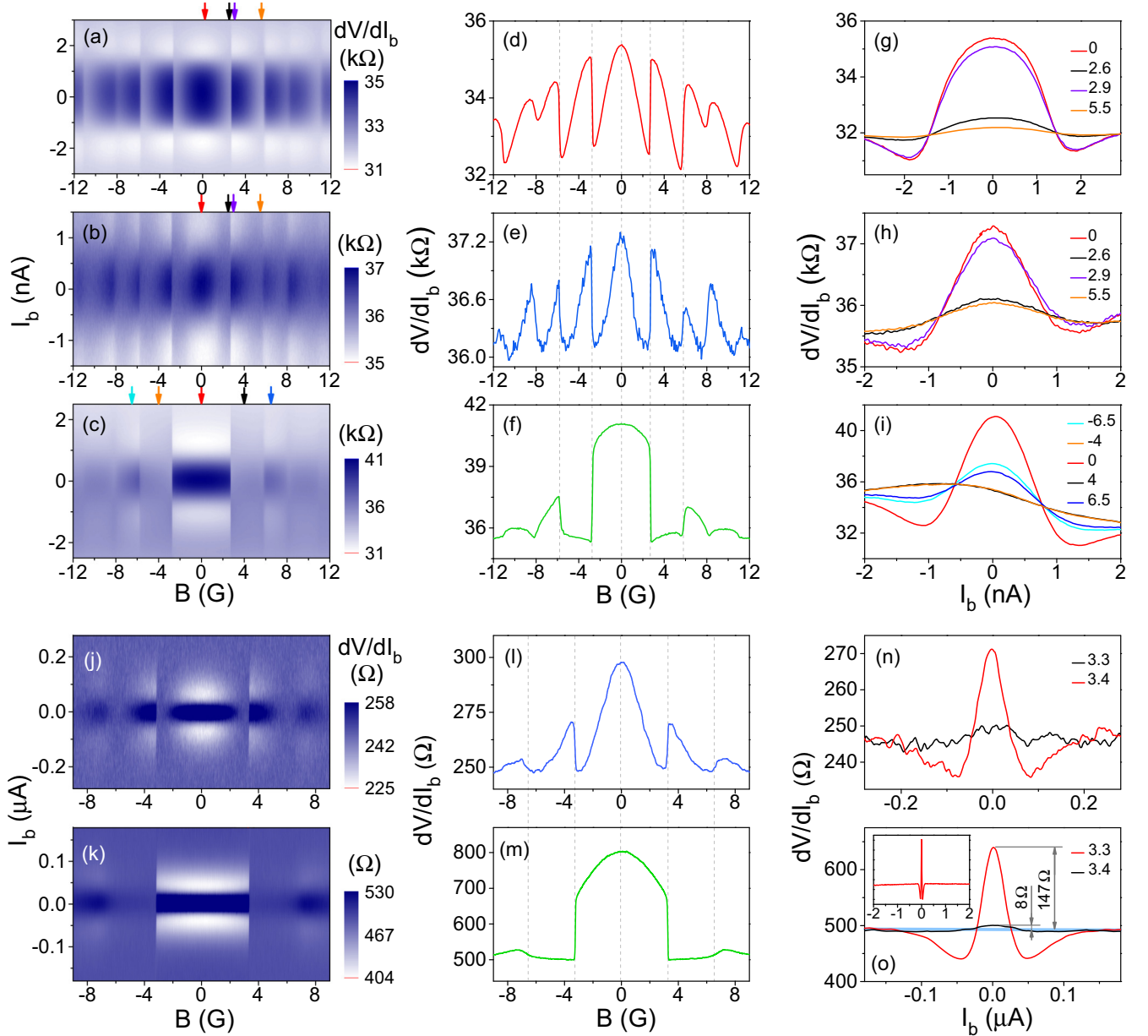


FIG. 3. The contact resistance dV/dI_b of devices 1 and 2 at ~ 20 mK. (a)–(c) The 2D plots of dV/dI_b of device 1 at positions A, B, and C, respectively, as functions of magnetic field B and bias current I_b . (d)–(f) dV/dI_b as a function of B along the horizontal line cuts at $I_b = 0$ in (a), (b), and (c), respectively. (g)–(i) dV/dI_b as a function of I_b along the vertical line cuts in (a), (b), and (c), respectively, at magnetic fields indicated by the arrows of corresponding color in the 2D plots. The numbers in the legends are in the unit of Gauss. (j)–(o) Similar data obtained at one of the ends and the center of device 2. The inset in (o) shows the data over a much wider current (hence voltage) range.

full gap closing—the minigap remains significantly open even if the total transmission coefficient D is as high as 0.99 (the red curves).

The local phase difference $\varphi(\phi, x)$ in Eq. (1) is controlled by the magnetic flux in the junction area:

$$\varphi(\phi, x) = 2\pi \frac{x\phi}{W\phi_0} \pm \pi \text{int}\left(\frac{\phi}{\phi_0}\right), \quad (2)$$

where $\phi = BWH$ is the total magnetic flux in the junction of area WH , and x is defined from $-W/2$ to $W/2$. The first term in Eq. (2) is the local phase difference caused by magnetic

flux. The second term represents a π phase jump whenever the total flux in the junction crosses the nodes of the Fraunhofer pattern.

For the mechanism of π phase jump, it is well known that for single Josephson junctions there exists a phase offset φ_0 which can be self-adjusted to minimize the total energy. As can be seen in the Supplemental Material [31], in the flux range of the zeroth Fraunhofer peak, the lowest-energy state corresponds to the $\varphi_0 = 0$ state. But in the flux range of the first Fraunhofer peak, the lowest-energy state corresponds to the $\varphi_0 = \pm\pi$ state. A π phase jump will thus take place at the nodes of the Fraunhofer pattern.

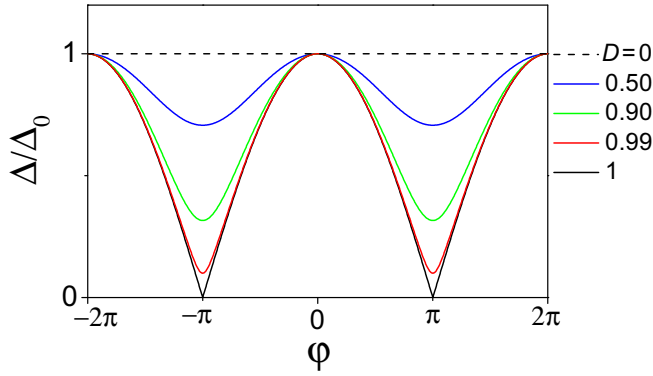


FIG. 4. The oscillations of minigap Δ with varying phase difference φ in S-N-S type Josephson junctions with different total transmission coefficient D .

B. Transparent or nontransparent? Dilemma and solution

As illustrated in Fig. 4, the minigap Δ is less oscillatory with varying magnetic flux when $D \rightarrow 0$ (the nontransparent limit), but becomes most oscillatory when $D \rightarrow 1$ (the transparent limit). The observation of significant dV/dI_b oscillation rules out that our Josephson junction is in the nontransparent limit—a conclusion which is in sharp contrast to the one drawn from the Fraunhofer pattern in Fig. 2. To solve this dilemma, we have to believe that there exist two distinct CPRs, corresponding to two different supercurrents as illustrated in Fig. 1(b). One CPR corresponds to the majority supercurrent flowing through the bulk of Bi_2Te_3 in the nontransparent limit [33], resulting in the measured Fraunhofer pattern of the nontransparent type. The other CPR corresponds to the supercurrent flowing through highly transparent channels, presumably the ABSs on the surface of Bi_2Te_3 . The contact resistance depends sensitively on the surface electron density of states, hence a highly oscillatory dV/dI_b was detected.

In the transparent limit $D = 1$, Eq. (1) becomes

$$\Delta = \Delta_0 |\cos(\varphi/2)|. \quad (3)$$

In this limit the minigap undergoes complete closing at the Fraunhofer nodes.

In the next sections we will analyze the data of the contact resistance quantitatively and qualitatively, to convince the readers that the minigap undergoes complete closing and that our Josephson junctions are indeed fully transparent.

C. Simulation of the dV/dI_b - I_b curves by using the BTK theory

Although the significant oscillation of the contact resistance infers that the Pb- Bi_2Te_3 -Pb Josephson junctions are in the transparent limit, the high value of the contact resistance itself tells that the transport process across the Pd- Bi_2Te_3 interface is rather nontransparent. We note that there was no intentionally made barrier at this interface. The remnant photoresist on the Bi_2Te_3 surface, if present, is ~ 1 nm thick or less as revealed by atomic force microscopy studies. Such an interface should allow the happening of direct tunneling of single quasiparticles as well as the two-particle Andreev reflection process. These processes are

usually described by the Blonder-Tinkham-Klapwijk (BTK) theory [34].

It is not quite straightforward that the BTK theory can be applied to describe the single-particle and two-particle processes across the Pd- Bi_2Te_3 interface here, since the superconducting gap in Bi_2Te_3 is not a standard one but an induced minigap between the lowest-energy electronlike and holelike Andreev bound states (or continuums in the dirty regime). Nevertheless, while the electronlike and holelike ABSs (or continuums) at the Bi_2Te_3 surface mediate the Josephson supercurrents between the two Pb electrodes, the same ABSs (or continuums) also define an energy window within which the two-particle process can occur between the Pd electrode and the superconducting bath (e.g., first to the superconducting bulk of Bi_2Te_3 [33], then eventually to the Pb electrodes). Although a rigorous theory is still needed to treat this special case, our numerical simulation below demonstrates that the BTK formalism works well to describe the single-particle and two-particle processes across the Pd- Bi_2Te_3 interface.

For a single conduction channel connecting a normal metal reservoir N and a superconductor reservoir S, the current can be expressed as

$$I = \frac{G_Q}{e} \int dE [1 - b(E) + a(E)] [f(E) - f(E - eV)], \quad (4)$$

where $G_Q = 2e^2/h$ is the quantum conductance, $b = r_{ee}^2$ is the normal (electron-to-electron) reflection coefficient to suppress the current, $a = r_{eh}^2$ is the Andreev (electron-to-hole) reflection coefficient to increase the current, and $f(E) = 1/[1 + \exp(E/k_B T)]$ is the Fermi distribution function of the left/right reservoirs.

According to the BTK theory:

$$1 - b(E) + a(E) = \begin{cases} \frac{2\Delta^2}{(eV)^2 + (1 + 2Z_{\text{Pd-TI}}^2) [\Delta^2 - (eV)^2]} & (eV < \Delta), \\ \frac{2eV}{eV + (1 + 2Z_{\text{Pd-TI}}^2) \sqrt{[(eV)^2 - \Delta^2]}} & (eV > \Delta), \end{cases} \quad (5)$$

where Δ is the minigap determined by the total transmission coefficient D of the Pb- Bi_2Te_3 -Pb Josephson junction via Eq. (1), and $Z_{\text{Pd-TI}}$ is the barrier strength of the Pd- Bi_2Te_3 interface, related to the transmission coefficient $D_{\text{Pd-TI}}$ of the interface via $D_{\text{Pd-TI}} = 1/(1 + Z_{\text{Pd-TI}}^2)$.

In the real case there exist multiple channels at the Pd- Bi_2Te_3 interface. For simplicity we assume that the transmission coefficient of each channel is the same. The total current is then

$$I = \frac{G_Q}{e} N \int dE [1 - b(E) + a(E)] [f(E) - f(E - eV)], \quad (6)$$

where N is the number of parallel channels.

With the above formula we can simulate the I - V curve, the dV/dI_b - V_b curve, as well as the dV/dI_b - I_b curve of the Pd- Bi_2Te_3 interface. Figure 5 shows the simulations on the dV/dI_b - I_b data of device 2 shown in Fig. 3(o). The fitting parameters are $Z_{\text{Pd-TI}} = 3.3$, $N = 670$, and $T = 50$ mK. The minigap is $9.25 \mu\text{eV}$ before closing at $B = 3.3$ G (the blue

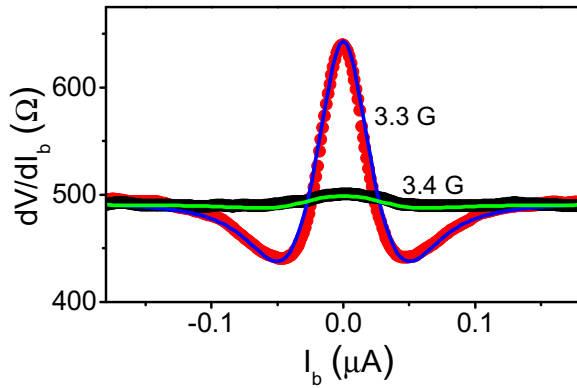


FIG. 5. Simulation of the dV/dI_b - I_b data measured by the central Pd electrode of device 2. The red and black symbols are the same data as shown in Fig. 3(o), and the blue and green lines are the simulations by assuming the Pd electrode is a geometric point. The parameters used in the simulations are: $T = 50$ mK, $Z_{\text{Pd-TI}} = 3.3$, $N = 670$, $\Delta_{3.3\text{G}} = 9.25$ μeV , and $\Delta_{3.4\text{G}} = 1.8$ μeV .

line), and 1.8 μeV after closing at $B = 3.4$ G (the green line). The large height reduction of the gap structure yields a very high transmission coefficient of $D = 1 - (\Delta/\Delta_0)^2 \approx 1 - (\Delta_{3.4\text{G}}/\Delta_{3.3\text{G}})^2 = 0.96$ for the Pb-Bi₂Te₃-Pb Josephson junction. This value of D is comparable to that of a single-atomic-layer Josephson junction [35] and an atomic superconducting point contact [36]. It is in sharp contrast to the transmission coefficient of the Pd-Bi₂Te₃ interface of the central Pd electrode in device 2, where $Z_{\text{Pd-TI}} = 3.3$ and hence the transmission coefficient is only $D_{\text{Pd-TI}} = 1/(1 + Z_{\text{Pd-TI}}^2) = 0.084$.

D. The finite-size effect of the Pd electrodes

In the above simulation we assume that the Pd electrode is a geometric point. In the real case, however, the Pd electrode always picks up signals within an area where the minigap remains unclosed at most places, such that the measured signature of gap closing is largely diminished. In other words, the true minigap at the center of the junction should be much smaller than 1.8 μeV when the magnetic flux reaches the Fraunhofer nodes. We therefore believe that the total transmission coefficient D of our S-TI-S junction is much higher than 0.96, being already in the fully transparent limit.

In the following we demonstrate that the remaining gap structure on the black/green curves in Fig. 5 can be well ascribed to the finite-size effect of the Pd electrode while complete gap closing already occurs at $x = 0$. From Eqs. (2) and (3) the position dependence of the minigap in the full transparent limit can be calculated. The results before and after the π phase jump in the vicinity of the first Fraunhofer node are plotted in Fig. 6. It can be seen that strict gap closing takes place only at the ends of the junction before the π phase jump, and at the center after the π phase jump. Obviously the central Pd electrode of device 2 with a width of ~ 800 nm illustrated by the light-blue rectangle in Fig. 6 picks up not

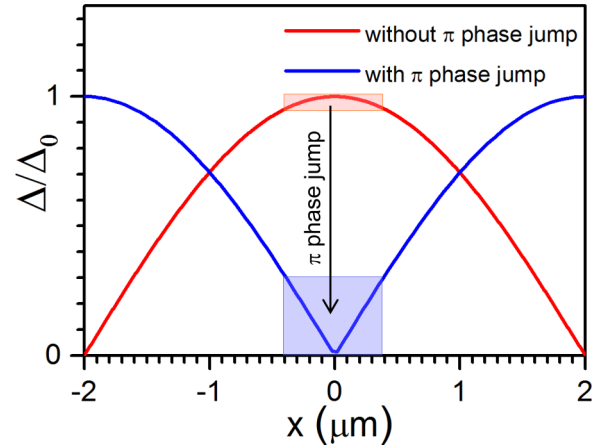


FIG. 6. The position dependence of minigap in a fully transparent junction at magnetic flux near the first Fraunhofer node. Red curve: Before π phase jump, i.e., $\phi = \phi_0^-$. Blue curve: After π phase jump, i.e., $\phi = \phi_0^+$. The width of the light-red and light-blue rectangles represents the diameter of the central Pd electrode along the x direction, and the heights of the rectangles indicate the ranges of minigap that the Pd electrode of a given width probes.

only the gap-closing signal at the center of the junction, but also the gap-opening signal in the vicinity area. Therefore, the measured signature of gap closing in real experiment is diminished by the finite size effect.

In Fig. 7 we show the dV/dI_b - I_b curves at $x = 0, \pm 200$, and ± 400 nm expected in the fully transparent limit, in comparison with the experimental data at $B = 3.4$ G taken from the central Pd electrode of device 2 whose diameter is ~ 800 nm. The results unambiguously show that the remaining tiny feature of gap in the experimental data can be a finite-size effect of the Pd electrode.

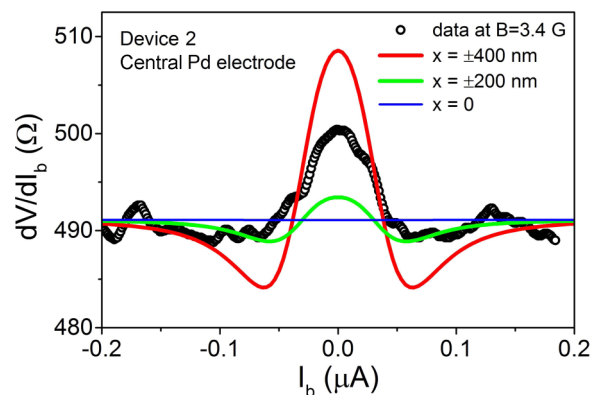


FIG. 7. Comparison between the remaining gap structure measured by the central Pd electrode of diameter $d = 800$ nm on device 2 at $B = 3.4$ G and the calculated ones at positions $x = 0, \pm 200$, and ± 400 nm, assuming the Pd-Bi₂Te₃-Pb junction is in the fully transparent limit. The other parameters used in the calculation are the same as in Fig. 5: $T = 50$ mK, $Z_{\text{Pd-TI}} = 3.3$, $N = 670$, and $\Delta_0 \approx \Delta_{3.3\text{G}} = 9.25$ μeV .

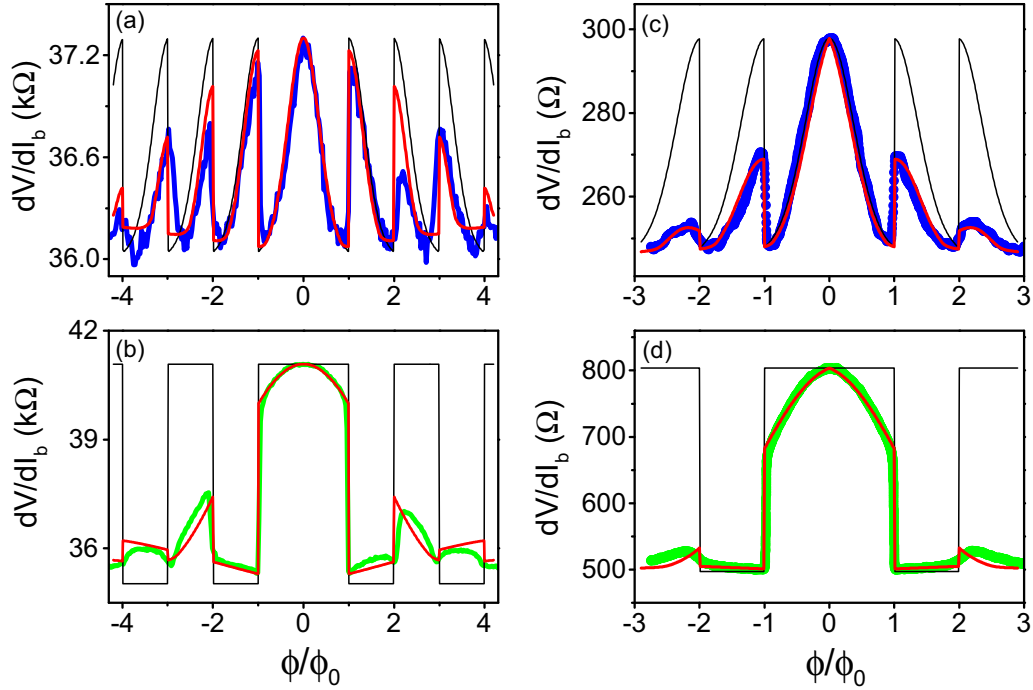


FIG. 8. Simulations of the magnetic flux dependence of dV/dI_b in the fully transparent limit. The black lines are the simulations without considering the size effect of the Pd electrodes. The red lines are the simulations after considering the size effect. (a) Simulating the data in Fig. 3(e) with parameters $T = 50$ mK, $Z_{\text{Pd-TI}} = 6.5$, $N = 21$, $\Delta_0 = 12$ μeV . The diameter of the side Pd electrode in device 1 is $d = 600$ nm. (b) Simulating the data in Fig. 3(f) with parameters $T = 50$ mK, $Z_{\text{Pd-TI}} = 6.9$, $N = 19$, $\Delta_0 = 10.3$ μeV . The diameter of the central Pd electrode in device 1 is $d = 660$ nm. (c) Simulating the data in Fig. 3(l) with parameters $T = 50$ mK, $Z_{\text{Pd-TI}} = 2.1$, $N = 550$, $\Delta_0 = 12$ μeV . The diameter of the side Pd electrode in device 2 is $d = 770$ nm. (d) Simulating the data in Fig. 3(m) with parameters $T = 50$ mK, $Z_{\text{Pd-TI}} = 3.3$, $N = 670$, $\Delta_0 = 12$ μeV . The diameter of the central Pd electrode in device 2 is $d = 800$ nm.

E. Simulations of the magnetic flux dependencies of zero-bias dV/dI_b in the fully transparent limit and after taking into account the finite-size effect of the Pd electrodes

Taking the finite-size effect of the Pd electrodes into account, we can further simulate the magnetic flux dependence of the data in the fully transparent limit $D = 1$.

Because the superconducting gap underneath the Pd electrode varies specially, the normal-reflection coefficient b and the Andreev-reflection coefficient a are functions of position x . The total current can be rewritten as

$$I = \frac{G_Q}{e} \int n(x) dx \int dE [1 - b(E) + a(E)] [f(E) - f(E - eV)], \quad (7)$$

where $n(x)$ is the number of channels per unit area (i.e., channel density). For simplicity we assume the channel density is a constant n_0 . The formula becomes

$$I = \frac{G_Q}{e} n_0 \int dx \int dE [1 - b(E) + a(E)] [f(E) - f(E - eV)]. \quad (8)$$

With Eqs. (5) and (8), the magnetic field dependence of dV/dI_b can be simulated. Plotted in Figs. 8(a)–8(d) are the simulations to the experimental data shown in Figs. 3(e), 3(f), 3(l), and 3(m), respectively. The blue and green dots are the experimental data. The black lines are the simulations assuming zero-sized electrodes located strictly at $x = \pm W/2$

(the ends) or $x = 0$ (the center). The red lines in Figs. 8(a) and 8(b) are the simulations for electrodes of diameter 600 nm at the end and 660 nm at the center of device 1, respectively. And the red lines in Figs. 8(c) and 8(d) are the simulations for electrodes of diameter ~ 770 nm at the end and ~ 800 nm at the center of device 2, respectively. The excellent agreement between the data and the simulations supports the conclusion that the Pb-Bi₂Te₃-Pb junctions are in the fully transparent limit, and that complete gap closing indeed occurs.

F. Further discussions

The total transmission coefficient D of an Pb-TI-Pb Josephson junction relies on the transmission coefficients of the two Pb-TI interfaces and that of the TI part. Although in this experiment we did not measure the barrier strength $Z_{\text{TI-Pb}}$ of single Bi₂Te₃-Pb interfaces, our early study on Bi₂Se₃-Sn interfaces prepared via the same techniques shows that the barrier strength is not close to 0 at all, but remains as high as 0.6 even after additional reactive ion etching was applied to reduce the remnant photoresist [13]. If taking $Z_{\text{TI-Pb}} = 0.6$, single Bi₂Te₃-Pb interface yields a transmission coefficient of $\sim 1/(0.6^2 + 1) = 0.74$, being already significantly smaller than 1. In addition to the interface scattering, the Bi₂Te₃ part in our junction is 1 μm in length. We therefore conclude that full transparency of quasiparticle transport in our Pb-Bi₂Te₃-Pb junctions could hardly be observed if without a mechanism to prohibit the happening of backscatterings. It

is due to the single-helicity nature of the surface states that the backscatterings are completely suppressed and perfect Andreev reflections are enabled between the two Bi_2Te_3 -Pd interfaces, leading to the formation of MZMs when π phase difference is reached. In contrast, the charge transport along the perpendicular direction across the Pd- Bi_2Te_3 interface has nothing to do with the zero mode formation, and thus is not protected to be fully transparent. In fact, the barrier strength $Z_{\text{Pd-TI}}$ of single Pd- Bi_2Te_3 interface ranges from 2.1 to 6.9 in this experiment (see the parameters in Fig. 8). Taking the central Pd electrode of device 2 as an example, whose $Z_{\text{Pd-TI}} = 3.3$, its transmission coefficient is only $1/(Z_{\text{Pd-TI}}^2 + 1) = 0.084$.

IV. SUMMARY

We have performed contact resistance measurement on single Josephson junctions constructed on Bi_2Te_3 surface. Complete gap closing is inferred from the data, indicating the existence of topologically protected full transparency of charge transport through the surface states of Bi_2Te_3 . Our results support the Fu-Kane proposal that Majorana zero modes can be hosted in Josephson junctions constructed on

the 2D surface of 3D TIs. Based on such a 2D platform, universal topological quantum computation could be further implemented [37].

Note added. The first version of this paper was posted on arXiv (arXiv:1603.04540). During revision we noticed that a similar work was recently carried out by Schüffelgen and co-workers [38], in which the authors show that for a Nb- Bi_2Te_3 -Nb Josephson junction containing a few tens nm of Bi_2Te_3 in length, the total transmission coefficient is as high as 0.95.

ACKNOWLEDGMENTS

We would like to thank L. Fu, G. M. Zhang, T. Xiang, X. C. Xie, Q. F. Sun, R. Du, Z. Fang, X. Dai, X. Hu, and Z. G. Cheng for fruitful discussions. This work was supported by the National Basic Research Program of China from the MOST Grants 2016YFA0300601, 2017YFA0304700, 2015CB921402, 2011CB921702, and 2009CB929101, by NSFC Grants 11527806, 91221203, 11174340, 11174357, 91421303, and 11774405, and by the Strategic Priority Research Program B of the Chinese Academy of Sciences Grant No. XDB07010100.

Z.L., Y.P., and J.W. contributed equally to this work.

-
- [1] E. Majorana, *Nuovo Cimento* **14**, 171 (1937).
 - [2] F. Wilczek, *Nat. Phys.* **5**, 614 (2009).
 - [3] R. F. Service, *Science* **332**, 193 (2011).
 - [4] M. Franz, *Physics* **3**, 24 (2010); *Nat. Nanotechnol.* **8**, 149 (2013).
 - [5] V. Mourik, K. Zuo, S. M. Frolov, S. R. Plissard, E. P. A. M. Bakkers, and L. P. Kouwenhoven, *Science* **336**, 1003 (2012).
 - [6] M. T. Deng, C. L. Yu, G. Y. Huang, M. Larsson, P. Caroff, and H. Q. Xu, *Nano Lett.* **12**, 6414 (2012).
 - [7] A. Das, Y. Ronen, Y. Most, Y. Oreg, M. Herblum, and H. Shtrikman, *Nat. Phys.* **8**, 887 (2012).
 - [8] H. O. H. Churchill, V. Fatemi, K. Grove-Rasmussen, M. T. Deng, P. Caroff, H. Q. Xu, and C. M. Marcus, *Phys. Rev. B* **87**, 241401 (2013).
 - [9] A. D. K. Finck, D. J. Van Harlingen, P. K. Mohseni, K. Jung, and X. Li, *Phys. Rev. Lett.* **110**, 126406 (2013).
 - [10] S. Nadj-Perge, I. K. Drozdov, J. Li, H. Chen, S. Jeon, J. Seo, A. H. MacDonald, B. A. Bernevig, and A. Yazdani, *Science* **346**, 602 (2014).
 - [11] S. Sasaki, M. Kriener, K. Segawa, K. Yada, Y. Tanaka, M. Sato, and Y. Ando, *Phys. Rev. Lett.* **107**, 217001 (2011).
 - [12] M. T. Deng, S. Vaitiekėnas, E. B. Hansen, J. Danon, M. Leijnse, K. Flensberg, J. Nygård, P. Krogstrup, and C. M. Marcus, *Science* **354**, 1557 (2016).
 - [13] F. Yang, Y. Ding, F. Qu, J. Shen, J. Chen, Z. Wei, Z. Ji, G. Liu, J. Fan, C. Yang, T. Xiang, and L. Lu, *Phys. Rev. B* **85**, 104508 (2012).
 - [14] L. P. Rokhinson, X. Liu, and J. K. Furdyna, *Nat. Phys.* **8**, 795 (2012).
 - [15] J. Wiedenmann, E. Bocquillon, R. S. Deacon, S. Hartinger, O. Herrmann, T. M. Klapwijk, L. Maier, C. Ames, C. Brüne, C. Gould, A. Oiwa, K. Ishibashi, S. Tarucha, H. Buhmann, and L. W. Molenkamp, *Nat. Commun.* **7**, 10303 (2016).
 - [16] S. P. Lee, K. Michaeli, J. Alicea, and A. Yacoby, *Phys. Rev. Lett.* **113**, 197001 (2014).
 - [17] I. Sochnikov, L. Maier, C. A. Watson, J. R. Kirtley, C. Gould, G. Tkachov, E. M. Hankiewicz, C. Brüne, H. Buhmann, L. W. Molenkamp, and K. A. Moler, *Phys. Rev. Lett.* **114**, 066801 (2015).
 - [18] C. Kurter, A. D. K. Finck, Y. S. Hor, and D. J. Van Harlingen, *Nat. Commun.* **6**, 7130 (2015).
 - [19] Y. Pang, J. Wang, Z. Z. Lyu, G. Yang, J. Fan, G. T. Liu, Z. Q. Ji, X. N. Jing, C. L. Yang, and L. Lu, *Chin. Phys. B* **25**, 117402 (2016).
 - [20] A. Yu Kitaev, *Phys. Usp.* **44**, 131 (2001).
 - [21] H. J. Kwon, V. M. Yakovenko, and K. Sengupta, *Low Temp. Phys.* **30**, 613 (2004).
 - [22] L. Fu and C. L. Kane, *Phys. Rev. B* **79**, 161408 (2009).
 - [23] R. M. Lutchyn, J. D. Sau, and S. Das Sarma, *Phys. Rev. Lett.* **105**, 077001 (2010).
 - [24] M. Diez, I. C. Fulga, D. I. Pikulin, M. Wimmer, A. R. Akhmerov, and C. W. J. Beenakker, *Phys. Rev. B* **87**, 125406 (2013).
 - [25] B. J. Wieder, F. Zhang, and C. L. Kane, *Phys. Rev. B* **89**, 075106 (2014).
 - [26] C. W. J. Beenakker, D. I. Pikulin, T. Hyart, H. Schomerus, and J. P. Dahlhaus, *Phys. Rev. Lett.* **110**, 017003 (2013).
 - [27] L. Fu and C. L. Kane, *Phys. Rev. Lett.* **100**, 096407 (2008).
 - [28] A. C. Potter and L. Fu, *Phys. Rev. B* **88**, 121109 (2013).
 - [29] H. Zhang, C.-X. Liu, S. Gazibegovic, D. Xu, J. A. Logan, G. Wang, N. van Loo, J. D. S. Bommer, M. W. A. de Moor, D. Car, R. L. M. O. het Veld, P. J. van Veldhoven, S. Koelling, M. A. Verheijen, M. Pendharkar, D. J. Pennachio, B. Shojaei, J. S. Lee, C. J. Palmstrøm, E. P. A. M. Bakkers, S. Das Sarma, L. P. Kouwenhoven, *Nature* **556**, 74 (2018).

- [30] M. Ebel, C. Busch, U. Merkt, M. Grajcar, T. Plecenik, and E. Il'ichev, *Phys. Rev. B* **71**, 052506 (2005).
- [31] See Supplemental Material at <http://link.aps.org/supplemental/10.1103/PhysRevB.98.155403> for more discussions.
- [32] C. W. J. Beenakker, *Transport Phenomena in Mesoscopic Systems*, edited by H. Fukuyama and T. Ando (Springer, Berlin, 1992).
- [33] F. Qu, F. Yang, J. Shen, Y. Ding, J. Chen, Z. Q. Ji, G. T. Liu, J. Fan, X. N. Jing, C. L. Yang, and L. Lu, *Sci. Rep.* **2**, 339 (2012).
- [34] G. E. Blonder, M. Tinkham, and T. M. Klapwijk, *Phys. Rev. B* **25**, 4515 (1982).
- [35] G. H. Lee, S. Kim, S. H. Jhi, and H. J. Lee, *Nat. Commun.* **6**, 6181 (2015).
- [36] M. L. Della Rocca, M. Chauvin, B. Huard, H. Pothier, D. Esteve, and C. Urbina, *Phys. Rev. Lett.* **99**, 127005 (2007).
- [37] S. Vijay, T. H. Hsieh, and L. Fu, *Phys. Rev. X* **5**, 041038 (2015).
- [38] P. Schüffelgen, Da. Rosenbach, C. Li, T. Schmitt, M. Schleenvoigt, A. R. Jalil, J. Kölzer, M. Wang, B. Bennemann, Um. Parlak, L. Kibkalo, M. Luysberg, G. Mussler, A. A. Golubov, A. Brinkman, T. Schäpers, and D. Grützmacher, [arXiv:1711.01665](https://arxiv.org/abs/1711.01665).